Available online at www.sciencedirect.com
SCIENCE DIRECT®
Journal of Solid State Chemistry 177 (2004) 3640–3649
JOURNAL OF SOLID STATE CHEMISTRY
http://elsevier.com/locate/jssc

Quaternary selenostannates $Na_{2-x}Ga_{2-x}Sn_{1+x}Se_6$ and $AGaSnSe_4$ (A = K, Rb, and Cs) through rapid cooling of melts. Kinetics versus thermodynamics in the polymorphism of $AGaSnSe_4$

Seong-Ju Hwang,[1] Ratnasabapathy G. Iyer, and Mercouri G. Kanatzidis*

Department of Chemistry, Center for Fundamental Materials Research, Michigan State University, 320 Chemistry Bldg., East Lansing, MI 48824, USA

Received 30 January 2004; accepted 9 June 2004

Available online 21 August 2004

Abstract

The quaternary alkali-metal gallium selenostannates, $Na_{2-x}Ga_{2-x}Sn_{1+x}Se_6$ and $AGaSnSe_4$ (A = K, Rb, and Cs), were synthesized by reacting alkali-metal selenide, Ga, Sn, and Se with a flame melting–rapid cooling method. $Na_{2-x}Ga_{2-x}Sn_{1+x}Se_6$ crystallizes in the non-centrosymmetric space group $C2$ with cell constants $a = 13.308(3)$ Å, $b = 7.594(2)$ Å, $c = 13.842(3)$ Å, $\beta = 118.730(4)^\circ$, $V = 1226.7(5)$ Å^3. α-$KGaSnSe_4$ crystallizes in the tetragonal space group $I4/mcm$ with $a = 8.186(5)$ Å and $c = 6.403(5)$ Å, $V = 429.1(5)$ Å^3. β-$KGaSnSe_4$ crystallizes in the space group $P2_1/c$ with cell constants $a = 7.490(2)$ Å, $b = 12.578(3)$ Å, $c = 18.306(5)$ Å, $\beta = 98.653(5)^\circ$, $V = 1705.0(8)$ Å^3. The unit cell of isostructural $RbGaSnSe_4$ is $a = 7.567(2)$ Å, $b = 12.656(3)$ Å, $c = 18.277(4)$ Å, $\beta = 95.924(4)^\circ$, $V = 1741.1(7)$ Å^3. $CsGaSnSe_4$ crystallizes in the orthorhombic space group $Pmcn$ with $a = 7.679(2)$ Å, $b = 12.655(3)$ Å, $c = 18.278(5)$ Å, $V = 1776.1(8)$ Å^3. The structure of $Na_{2-x}Ga_{2-x}Sn_{1+x}Se_6$ consists of a polar three-dimensional network of trimeric $(Sn,Ga)_3Se_9$ units with Na atoms located in tunnels. The $AGaSnSe_4$ possess layered structures. The compounds show nearly the same Raman spectral features, except for $Na_{2-x}Ga_{2-x}Sn_{1+x}Se_6$. Optical band gaps, determined from UV–Vis spectroscopy, range from 1.50 eV in $Na_{2-x}Ga_{2-x}Sn_{1+x}Se_6$ to 1.97 eV in $CsGaSnSe_4$. Cooling of the melts of $KGaSnSe_4$ and $RbGaSnSe_4$ produces only kinetically stable products. The thermodynamically stable product is accessible under extended annealing, which leads to the so-called γ-form ($BaGa_2S_4$-type) of these compounds.

Keywords: Selenostannates; Polymorphism; Frame melting; Chalcogenicles; Low-dimensional; Phase-transitions

1. Introduction

The structural chemistry of complex chalcogenides containing tetravalent group 14 elements (i.e., Si, Ge, Sn) has been relatively well investigated [1–3]. Due to the strong preference of these elements for tetrahedral geometry, most compounds possess crystal structures consisting of a variety of edge- or corner-shared MQ_4 (M = Si, Ge, Sn; Q = S, Se, Te) tetrahedra. These include (i) $[MQ_4]^{4-}$ tetrahedra [4,5], (ii) the $[M_2Q_7]^{6-}$ unit formed by the corner-sharing of two tetrahedra [6], (iii) the adamantane-like $[M_4Q_{10}]^{4-}$ unit formed by the sharing of three corners of each tetrahedron [7], and (iv) the $[M_2Q_6]^{4-}$ dimers formed by the edge-sharing of two tetrahedra [8]. Several quaternary selenostannates are known with transition metals such as Cu, Ag, Au, and Mn [9,10].

Fewer reports exist with group 13 elements (e.g., Al, Ga, and In). From the viewpoint of synthetic methodology, selenostannates have been generally prepared in flux medium at intermediate temperature or by direct combination reactions followed by slow cooling to achieve crystallization. The latter technique results in thermodynamically stable phases in the range of crystallization temperature. In an attempt to avoid thermodynamically stable phases and favor kinetically stable or even metastable phases we opted to take the exact opposite approach. That is a fast reaction, followed by

*Corresponding author. Fax: +517-353-1793.
E-mail address: kanatzid@cem.msu.edu (M.G. Kanatzidis).
[1] Present address: Department of Applied Chemistry, Center for Optoelectronics and Microwave Thin-Film Devices, College of Natural Sciences, Konkuk University Chungju Campus, Chungju, Chungbuk 380-701, South Korea.

0022-4596/$ - see front matter © 2004 Elsevier Inc. All rights reserved.
doi:10.1016/j.jssc.2004.06.019

rapid quenching to induce rapid crystallization. In this regard, we have explored a flame melting–rapid cooling method in which the reactants are thoroughly melted by a torch flame and then rapidly quenched into room temperature or even liquid N_2 temperature. This approach can produce cooling rates in the order of 200°C/min and can be useful (although it does not guarantee) in accessing kinetically stable phases that cannot be prepared by conventional slow cooling processes. Such a tactic has been little exploited. Recently, we reported some interesting metastable compounds (e.g., $KBiP_2Se_6$ and $KSbP_2Se_6$) [11], KSb_5S_8 [12], and β-$KInSnSe_4$ [13] that have been trapped through rapid melt cooling. These materials exhibit phase transitions to more thermodynamically stable configurations simply by annealing below the melting point.

Here we report several quaternary alkali-metal gallium selenostannates synthesized through this flame melting–rapid cooling method, and also describe their crystal structures and optical properties. $Na_{2-x}Ga_{2-x}Sn_{1+x}Se_6$ (**I**) has a three-dimensional framework structure consisting of trimeric $(Sn,Ga)_3Se_9$ units and tunnels where the Na atoms reside. The structures of $KGaSnSe_4$ (**II**), $RbGaSnSe_4$ (**III**), and $CsGaSnSe_4$ (**IV**) are layered in which one-dimensional chains consisting of edge-shared $(Sn,Ga)_2Se_6$ dimers and $(Sn,Ga)Se_4$ tetrahedra are linked side-by-side. We show that in $KGaSnSe_4$, $RbGaSnSe_4$, cooling of the melts does not produce the thermodynamically stable product. In fact the latter is inaccessible under melt-cooling conditions; instead a proper solid-state annealing protocol is necessary to obtain the so-called γ-form of these compounds. The implications of these results are discussed.

2. Experimental

Chemicals were used as obtained without further purification: (i) Ga metal (3 mm shots 99.999%, CERAC, Inc.) (ii) Sn metal (99.8%, −325 mesh, CERAC, Inc.), and (iii) Se (99.99%, Noranda Advanced Materials, Quebec, Canada) A_2Se (A = Na, K, Rb, and Cs) were prepared by reaction of stoichiometric amounts of alkali-metal and selenium in liquid ammonia [14]. All manipulations were carried out under a dry nitrogen atmosphere inside a glovebox.

Red crystals of $Na_{2-x}Ga_{2-x}Sn_{1+x}Se_6$ (**I**), yellowish-brown needles and reddish-orange crystals of α- and β-$KGaSnSe_4$ (**II**), respectively, reddish-orange crystals of $RbGaSnSe_4$ (**III**), and reddish-orange crystals of $CsGaSnSe_4$ (**IV**) were synthesized by the stoichiometric reaction of A_2Se (A = Na, K, Rb, and Cs), Ga, Sn, and Se with the ratio of A:Ga:Sn:Se = 1:1:1:4. For each system the starting materials were loaded into a fused silica tube and sealed under vacuum. The starting materials were thoroughly melted in a torch flame and then the liquid was allowed to rapidly cool in air. This corresponds to ∼200°C/min cooling rate. For **II**, **III**, and **IV** pure phases were obtained. In the case of **I** transparent plate crystals were isolated in ∼50% yield. Semiquantitative energy dispersive spectroscopic (EDS) microprobe analysis on several single crystals confirmed the formation of quaternary phases.

Selected single crystals were affixed to a metal plate using carbon tape. Semiquantitative microprobe analyses were performed with a JEOL JSM-35C scanning electron microscope (SEM) equipped with a Tracor Northern energy-dispersive spectroscope (EDS) detector. Data acquisitions were performed using an accelerating voltage of 20 kV and a 30 s accumulation time.

Raman spectra were recorded using a BIO-RAD FT Raman spectrometer with a Spectra-Physics Topaz T10–106c laser.

The band gap energy values were extracted from UV–Vis diffuse reflectance spectra obtained on a Shimadzu UV-3101PC double-beam, double-monochromator spectrophotometer in the wavelength range 200–2500 nm using a protocol described elsewhere [15].

Differential thermal analysis (DTA) was performed on a computer-controlled Shimadzu DTA-50 thermal analyzer. Typically, 20–30 mg of selected crystals were sealed in a quartz ampoule under vacuum. The ampoule was heated to 800°C at 10°C/min and isothermed for 1 min followed by cooling at −10°C/min to 100°C. The sample stability and congruent melting was monitored by running a second heating/cooling cycle. In order to probe a possibility of phase change during DTA, powder XRD patterns were measured for the samples before and after the experiment using X-ray Cu$K\alpha$ radiation with a graphite monochromator.

Single crystals were mounted on glass fibers and crystallographic data corresponding to a hemisphere of reciprocal space were collected on a Siemens Platform SMART CCD diffractometer using a graphite monochromator and Mo$K\alpha$ ($\lambda = 0.71073$ Å) radiation. The SMART [16] software was used for data acquisition and cell reduction, and the integration was done with the SAINT software package. The face-indexing routine was applied for analytical absorption corrections. Empirical absorption corrections were also done with SADABS. The structure solution was accomplished by direct methods and refinements were performed with the SHELXTL software package. Since $KGaSnSe_4$ and $RbGaSnSe_4$ were found to be isostructural, we focused on $KGaSnSe_4$ as being representative. We also found after complete refinement that there were deviations from the ideal stoichiometries. The refinements indicated $A_{1-x}Ga_{1+x}Sn_{1-x}Se_4$ ($x < 0.04$). Nevertheless, except for the Na salt in which the deviations are more substantial, we will refer to these compounds with their ideal stoichiometry. The crystallographic data for all present compounds are summarized in Table 1, and

Table 1
Crystallographic data collection and refinement parameters

Formula	$Na_{7.36}Ga_{7.24}Sn_{4.78}Se_{24}$	$K_{7.968}Ga_{8.3}Sn_{7.7}Se_{32}$	$Rb_8Ga_{7.36}Sn_{8.64}Se_{32}$	$Cs_{7.89}Ga_{8.38}Sn_{7.62}Se_{32}$
Fw	3136.22	4331.21	4748.80	5064.27
Space group	*C*2	$P2_1/c$	$P2_1/c$	*Pmcn*
a (Å)	13.308(3)	7.490(2)	7.567(2)	7.679(2)
b (Å)	7.594(2)	12.578(3)	12.656(3)	12.655(3)
c (Å)	13.842(3)	18.306(5)	18.277(4)	18.278(5)
β (deg)	118.730(4)	98.653(5)	95.924(4)	—
V (Å^3)	1226.6(5)	1705.0(8)	1741.1(7)	1776.1(8)
Z	1	1	1	1
Calcd density (g/cm^3)	4.246	4.218	4.529	4.735
μ (mm^{-1})	24.170	23.561	28.124	26.139
λ (Å)	0.71073	0.71073	0.71073	0.71073
θ range for data collection (deg)	1.68–28.21	3.24–28.34	3.33–28.29	1.96–28.10
Temp (K)	293	293	293	293
R indices	R_1[a] = 0.0417	R_1[a] = 0.0379	R_1[a] = 0.0778	R_1[a] = 0.0442
($I > 2\sigma(I)$)	wR_2[b] = 0.1088	wR_2[b] = 0.0823	wR_2[b] = 0.2294	wR_2[b] = 0.0951
R indices	R_1[a] = 0.0493	R_1[a] = 0.0657	R_1[a] = 0.1236	R_1[a] = 0.0957
(All data)	wR_2[b] = 0.1119	wR_2[b] = 0.0894	wR_2[b] = 0.2478	wR_2[b] = 0.1123
GOF on F^2	1.062	0.893	1.085	0.919

[a] $R_1 = \sum(|F_o| - |F_c|)/\sum|F_o|$.
[b] $wR_2 = \{\sum w(|F_o| - |F_c|)^2/\sum w|F_o|\}^{2}\}^{1/2}$.

Table 2
Atomic positions and equivalent isotropic displacement parameters (Å^2) for $Na_{2-x}Ga_{2-x}Sn_{1+x}Se_6$

Atom	Wyckoff position	*x*	*y*	*z*	U_{eq}	Occupancy of Sn/Ga
M(1)	4*c*	0.2666(1)	0.6571(1)	0.2722(1)	0.025(1)	0.47(1)/0.53(1)
M(2)	4*c*	0.4943(1)	0.9071(1)	0.2276(1)	0.025(1)	0.49(1)/0.51(1)
M(3)	2*a*	0.5	0.9350(2)	0.5	0.026(1)	0.28(1)/0.72(1)
M(4)	2*b*	0	0.6851(2)	0	0.023(1)	0.18(1)/0.82(1)
Se(1)	4*c*	0.4211(1)	0.6061(2)	0.2265(1)	0.032(1)	1
Se(2)	4*c*	0.1191(1)	0.8707(2)	0.1561(1)	0.031(1)	1
Se(3)	4*c*	0.1947(1)	0.3562(2)	0.2737(1)	0.032(1)	1
Se(4)	4*c*	0.4629(1)	1.1206(2)	0.3441(1)	0.031(1)	1
Se(5)	4*c*	0.3342(1)	0.7554(2)	0.4631(1)	0.036(1)	1
Se(6)	4*c*	0.3708(1)	1.0057(2)	0.0368(1)	0.035(1)	1
Na(1)	4*c*	0.6205(9)	0.4339(15)	0.4040(12)	0.103(6)	1.00(3)
Na(2)	4*c*	0.2158(11)	1.1858(14)	0.0958(11)	0.080(5)	0.84(3)

fractional coordinates and isotropic thermal parameters are listed for **I**, **II** (β-), and **IV** in Tables 2–4, respectively. The cif files have been deposited with the ICSD data base, Fachinformationszentrum (FIZ) Karlsruhe. These can be accessed via depositions numbers CSD-413686 for $Na_{0.92}Ga_{0.90}Sn_{0.6}Se_3$, CSD-414109 for α-KGaSnSe$_4$, CSD-413685 for β-KGaSnSe$_4$, CSD-413683 for RbGaSnSe$_4$ and CSD-413684 for CsGaSnSe$_4$.

3. Results and discussion

3.1. Structure of $Na_{0.9}Ga_{0.9}Sn_{0.6}Se_3$

The Ga and Sn sites in the lattice are mixed occupancy sites and compared to the ideal composition of "NaGaSn$_{0.5}$Se$_3$" there exist a slight excess of tin atoms on metal sites *M*(1) and *M*(2). As a result, the concentration of Na and Ga is slightly decreased from the ideal concentration to maintain charge neutrality. As illustrated in Fig. 1, the structure of **I** is non-centrosymmetric and polar and contains a three-dimensional network of corner-shared (Sn, Ga)Se$_4$ tetrahedra. The network consists of trimeric (Sn,Ga)$_3$Se$_9$ units formed by three tetrahedra with sharing two corners each, see Fig. 2. There are two kinds of (Sn,Ga)$_3$Se$_9$ units, i.e., one is formed by (Sn, Ga)(1)Se$_4$(Sn, Ga)(2)Se$_4$(Sn, Ga)(3)Se$_4$ (denoted as *trimer 1*) and the other is formed by (Sn, Ga)(1)Se$_4$(Sn, Ga)(2)Se$_4$(Sn, Ga)(4)Se$_4$ (denoted as *trimer 2*). Each trimer contains a six-membered ring. Such a trimer has been found from Ba–Fe–S system [17]. The linking of three (Sn,Ga)$_3$Se$_9$ trimers creates 12-membered rings

Table 3
Atomic positions and equivalent isotropic displacement parameters (Å^2) for $KGaSnSe_4$

Atom	Wyckoff position	x	y	z	U_{eq}	Occupancy of Sn/Ga
$M(1)$	4e	0.2600(1)	0.7058(1)	0.1788(1)	0.025(1)	0.67(1)/0.33(1)
$M(2)$	4e	0.2942(1)	0.8186(1)	0.0159(1)	0.024(1)	0.69(1)/0.31(1)
$M(3)$	4e	0.5388(1)	0.7507(1)	0.3591(1)	0.023(1)	0.35(1)/0.65(1)
$M(4)$	4e	0.0248(1)	0.7520(1)	0.3407(1)	0.022(1)	0.21(1)/0.79(1)
Se(1)	4e	0.2811(1)	0.8709(1)	0.3469(1)	0.028(1)	1
Se(2)	4e	0.5096(1)	0.6184(1)	0.2602(1)	0.032(1)	1
Se(3)	4e	0.7863(1)	0.8767(1)	0.3560(1)	0.027(1)	1
Se(4)	4e	0.2496(1)	0.6275(1)	0.0508(1)	0.033(1)	1
Se(5)	4e	0.5967(1)	0.8459(1)	−0.0213(1)	0.032(1)	1
Se(6)	4e	0.0435(1)	0.8940(1)	−0.0719(1)	0.030(1)	1
Se(7)	4e	−0.0379(1)	0.6694(1)	0.2172(1)	0.034(1)	1
Se(8)	4e	0.3001(1)	0.8947(1)	0.1426(1)	0.034(1)	1
K(1)	4e	0.7600(4)	0.9003(2)	0.5473(1)	0.058(1)	0.99(1)
K(2)	4e	0.2248(4)	1.0692(2)	−0.1741(1)	0.066(1)	1.00(1)

Table 4
Atomic positions and equivalent isotropic displacement parameters (Å^2) for $CsGaSnSe_4$

Atom	Wyckoff position	x	y	z	U_{eq}	Occupancy of Sn/Ga
$M(1)$	4c	0.2500	0.8000(1)	0.1792(1)	0.024(1)	0.65(1)/0.35(1)
$M(2)$	4c	0.2500	0.6870(1)	0.0163(1)	0.022(1)	0.56(1)/0.44(1)
$M(3)$	8d	−0.0047(1)	0.7492(1)	0.3474(1)	0.021(1)	0.35(1)/0.65(1)
Se(1)	4c	0.2500	1.1253(1)	0.1507(1)	0.024(1)	1
Se(2)	4c	0.2500	0.6332(1)	0.3439(1)	0.027(1)	1
Se(3)	8d	0.0187(2)	0.3676(1)	0.0459(1)	0.028(1)	1
Se(4)	8d	−0.0179(2)	0.8640(1)	0.2389(1)	0.031(1)	1
Se(5)	4c	0.2500	0.6105(1)	0.1420(1)	0.032(1)	1
Se(6)	4c	0.2500	0.8767(1)	0.0519(1)	0.028(1)	1
Cs(1)	4c	0.2500	0.4301(1)	−0.1522(1)	0.043(1)	0.98(1)
Cs(2)	4c	−0.2500	0.8784(1)	0.0532(1)	0.037(1)	0.99(1)

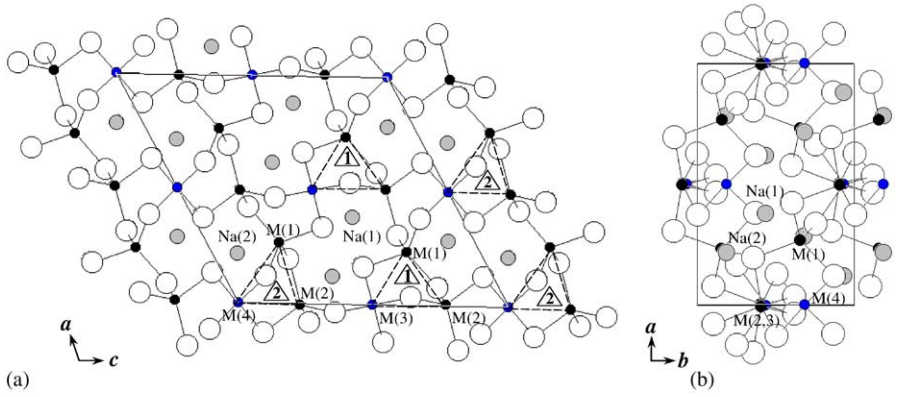

Fig. 1. Projections of the structure of $Na_{2-x}Ga_{2-x}Sn_{1+x}Se_6$ along the (a) b- and (b) c-axis showing the three-dimensional nature of the framework. The polar character of the structure, along the b-axis, is clearly observed in this view. Large open circles are Se atoms, black circles are 4-coordinate (Sn,Ga) atoms, and medium gray circles are Na atoms. The numbers in the dashed triangles represent the types of trimeric $(Sn,Ga)_3Se_9$ units. M represents disordered, mixed occupancy cation sites for Sn and Ga.

forming a tunnel along the [010] direction. Depending on orientation, two different kinds of 12-membered rings are created. One, oriented along the [001] direction, is formed by the connection of $trimer2-trimer2-trimer1$. The other, oriented along the [101] direction, forms by combining $trimer1-trimer1-trimer2$. There is one type of Na^+ site in each ring.

The tetrahedral geometry of the $(Sn,Ga)(1)Se_4$ and $(Sn,Ga)(2)Se_4$ units is rather distorted with the

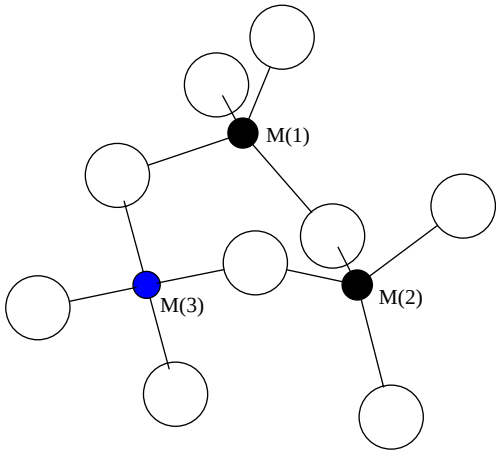

Fig. 2. Geometry of the corner-shared "$(Sn,Ga)_3Se_9$ trimer" found in $Na_{2-x}Ga_{2-x}Sn_{1+x}Se_6$. *M* represents disordered cation sites for Sn and Ga.

(Sn,Ga)–Se bond distances ranging from 2.456(1) to 2.480(2) Å for the site $M(1)$ and from 2.456(1) to 2.482(2) Å for the site $M(2)$ (see Table 5). The $Se-(Sn,Ga)-Se$ bond angles range from 102.35(7)° to 116.10(7)° for the site $M(1)$ and from 102.47(6)° to 116.02(7)° for the site $M(2)$. These values deviate somewhat from the bond angle of regular tetrahedra 109.5°. On the contrary, the $(Sn,Ga)(3)Se_4$ and $(Sn,Ga)(4)Se_4$ tetrahedra are less distorted. The $(Sn,Ga)-Se$ bond distances are 2.421(2) and 2.431(2) Å for the site $M(3)$ and 2.424(2) and 2.432(2) Å for $M(4)$. The $Se-(Sn,Ga)-Se$ bond angles show relatively small deviation from that of regular tetrahedra, i.e., 106.83(5)–111.74(12)° for the site $M(3)$ and from 106.71(5)° to 111.87(12)° for the site $M(4)$. Such a difference in the degree of structural distortion can be understood considering the occupancy of Sn versus Ga in each metal site. While the occupancy of Sn in sites $M(1)$ and $M(2)$ is nearly the same as that of Ga, sites $M(3)$ and $M(4)$ are occupied mostly by Ga atoms. This also explains the observed difference in average $(Sn,Ga)-Se$ bond distances, i.e., 2.464(2) Å for sites $M(1)$ and $M(2)$ and 2.427(2) Å for sites $M(3)$ and $M(4)$.

The Na atoms are coordinated by five Se atoms with Na–Se bond distances ranging from 2.892(11) to 3.457(15) Å for Na(1) and from 2.900(10) to 3.465(14) Å for Na(2). The five Se atoms form a severely distorted $[NaSe_5]^{9-}$ trigonal bipyramidal geometry.

The non-centrosymmetric character is straightforward to understand when focusing on the connection of the trimeric units. As shown in Fig. 1, the structure can be described by parallel alignment of corner-shared trimer chains along the [101] direction, i.e., *–trimer 1–trimer 2–trimer 1–trimer 2–*. Since all the chains are aligned in the same direction, no center of symmetry can be formed. The non-centrosymmetric, strongly polar character of this structure suggests the possibility of respectable non-linear optical property for this material.

3.2. Structure of $AGaSnSe_4$ (A=K, Rb, and Cs)

α-$KGaSnSe_4$ has chains composed of edge sharing $GaSe_4$ and $SnSe_4$ tetrahedra that run parallel to the *c*-axis. Sn and Ga occupy the same crystallographic site with a site occupancy factor of 50% each. This compound is isostructural to α-$KInSnSe_4$.[2]

β-$KGaSnSe_4$ (**II**), $RbGaSnSe_4$ (**III**), and $CsGaSnSe_4$ (**IV**) have layered structures with the layers oriented perpendicular to the [010] direction, Fig. 3. As in **I**, mixed site occupancy is observed between the Ga and Sn atoms which are present in tetrahedral sites. The gallium selenostannate layer is formed by the side-by-side linking of one-dimensional chains, Fig. 4. Depending on one's view two types of these chains can be identified. One type forms by corner-sharing of tetrameric $(Sn,Ga)_4Se_{11}$ units running along the [100] direction. On the other hand, along the [001] direction, another type of chain is recognizable formed by alternating edge-shared $(Sn,Ga)_2Se_6$ dimer units and $(Sn,Ga)Se_4$ tetrahedra, Fig. 5. This layered structure is found in $TlInSiS_4$ and $KGaSnS_4$ with space groups of *Pbnm* and $P\bar{1}$, respectively [18,19].

It is surprising that the flame melting–cooling method produced both the α- and β-forms of $KGaSnSe_4$. In the analogous $KInSnSe_4$ system, we obtained the α-phase from controlled slow cooling of the melt, whereas the β-form was obtained from the flame [13]. In the $KGaSnSe_4$ system, when we attempted a slow cooling of the melt in a furnace, we obtained the β-phase. This probably indicates that the thermodynamic and kinetic stabilities of the α- and the β-forms of $KGaSnSe_4$ are delicately balanced and a slight difference in the reaction conditions can lead to the formation of one over the other. Interestingly as we will show below both these forms are only kinetically stable.

The $[GaSnSe_4]^{1-}$ slabs are held through electrostatic interaction with interlayer alkali-metal ions. As the size of alkali-metal increases from K to Cs, the crystal symmetry increases. Namely, **IV** crystallizes with the orthorhombic symmetry whereas **II** and **III** have monoclinic symmetry. The larger Cs atoms interact equally with equivalent selenium atoms in adjacent chains running along the [001] direction and hence

[2] Crystal data for α-$KGaSnSe_4$ at 293K: $a = 8.186(5)$ Å, $c = 6.403(5)$ Å; tetragonal, $I4/mcm$; $Z = 4$; $V = 429.1(5)$ Å^3; $D = 8.411$ mg/m^3; $\mu = 46.799$ mm^{-1}; $F(000) = 944$; Total reflections/unique = 1671/161; $R_{int} = 0.04$; Data/parameters = 161/9; GoF on F^2 = 1.141; $R_1/wR_2(I > 2\sigma) = 3.31/7.27$. A complete list of atomic coordinates and temperature factors can be obtained from FIZ Karlsruhe by quoting CSD—414109.

Table 5
Selected interatomic distances (Å) and angles (deg) for $Na_{2-x}Ga_{2-x}Sn_{1+x}Se_6$

Atoms	Distance	Atoms	Distance
Sn,Ga(1)–Se(1)	2.456(1)	Sn,Ga(1)–Se(2)	2.457(2)
Sn,Ga(1)–Se(3)	2.480(2)	Sn,Ga(1)–Se(5)	2.462(2)
Sn,Ga(2)–Se(1)	2.482(2)	Sn,Ga(2)–Se(3)	2.456(1)
Sn,Ga(2)–Se(4)	2.460(2)	Sn,Ga(2)–Se(6)	2.462(2)
Sn,Ga(3)–Se(4)	2.421(2)	Sn,Ga(3)–Se(5)	2.431(2)
Sn,Ga(4)–Se(2)	2.424(2)	Sn,Ga(4)–Se(6)	2.432(2)
Na(1)–Se(1)	2.919(11)	Na(1)–Se(2)	3.457(15)
Na(1)–Se(4)	3.013(12)	Na(1)–Se(5)	2.892(11)
Na(1)–Se(5)	2.940(11)		
Na(2)–Se(2)	3.018(11)	Na(2)–Se(3)	2.913(11)
Na(2)–Se(4)	3.465(14)	Na(2)–Se(6)	2.900(10)
Na(2)–Se(6)	2.927(10)		
Atoms	**Angle**	**Atoms**	**Angle**
Se(1)–Sn,Ga(1)–Se(2)	116.10(7)	Se(1)–Sn,Ga(1)–Se(3)	103.36(7)
Se(1)–Sn,Ga(1)–Se(5)	113.91(7)	Se(2)–Sn,Ga(1)–Se(3)	115.05(7)
Se(2)–Sn,Ga(1)–Se(5)	105.47(7)	Se(3)–Sn,Ga(1)–Se(5)	102.35(7)
Se(1)–Sn,Ga(2)–Se(3)	103.35(7)	Se(1)–Sn,Ga(2)–Se(4)	114.91(7)
Se(1)–Sn,Ga(2)–Se(6)	102.47(6)	Se(3)–Sn,Ga(2)–Se(4)	116.02(7)
Se(3)–Sn,Ga(2)–Se(6)	114.07(7)	Se(4)–Sn,Ga(2)–Se(6)	105.46(7)
Se(4)–Sn,Ga(3)–Se(4)	108.81(11)	Se(4)–Sn,Ga(3)–e(5)	106.83(5)
Se(4)–Sn,Ga(3)–Se(5)	106.83(5)	Se(4)–Sn,Ga(3)–Se(5)	111.32(5)
Se(4)–Sn,Ga(3)–Se(5)	111.32(5)	Se(5)–Sn,Ga(3)–Se(5)	111.74(12)
Se(2)–Sn,Ga(4)–Se(2)	108.85(11)	Se(2)–Sn,Ga(4)–Se(6)	106.71(5)
Se(2)–Sn,Ga(4)–Se(6)	106.71(5)	Se(2)–Sn,Ga(4)–Se(6)	111.36(5)
Se(2)–Sn,Ga(4)–Se(6)	111.36(5)	Se(6)–Sn,Ga(4)–Se(6)	111.87(12)

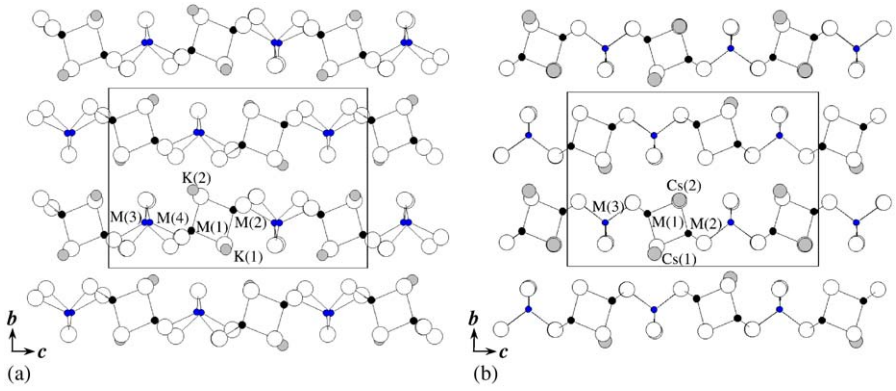

Fig. 3. Projections along the *a*-axis of: (a) $KGaSnSe_4$ and (b) $CsGaSnSe_4$, showing the stacking of the layers and placement of alkali-metal atoms. Large open circles are Se atoms, black circles are 4-coordinate (Sn,Ga) atoms, and medium gray circles are K or Cs atoms. *M* represents disordered sites for Sn and Ga.

decrease the β angle to 90°, giving orthorhombic symmetry, Fig. 4.

As evidenced from the bond distances and bond angles of **II** in Table 6, the tetrahedral coordination sphere around metal sites 1 and 2 in the dimeric $(Sn,Ga)_2Se_6$ unit are more distorted than those in the $(Sn,Ga)(3)Se_4$ and $(Sn,Ga)(4)Se_4$ tetrahedra. In the $(Sn,Ga)_2Se_6$ sites, half of coordinating Se atoms take part in edge-sharing with neighboring tetrahedra and the rest are shared by adjacent tetrahedra through corner-sharing. In contrast, all the Se atoms in $(Sn,Ga)(3)Se_4$ and $(Sn,Ga)(4)Se_4$ participate in the corner-sharing with neighboring tetrahedra. As a result, the difference among the (Sn,Ga)–Se bond distances is greater among the sites $M(1)$ and $M(2)$ than the sites $M(3)$ and $M(4)$ (see Table 6).

The bond angle of Se(bridging)–(Sn,Ga)–Se(bridging) is smaller than the other angles, which helps to decrease the electrostatic repulsion between adjacent (Sn^{+4},Ga^{+3}) centers in dimers. Similar trends in bond distances, bond angles, and metal occupancy are also observed in **IV**, see Tables 4 and 7.

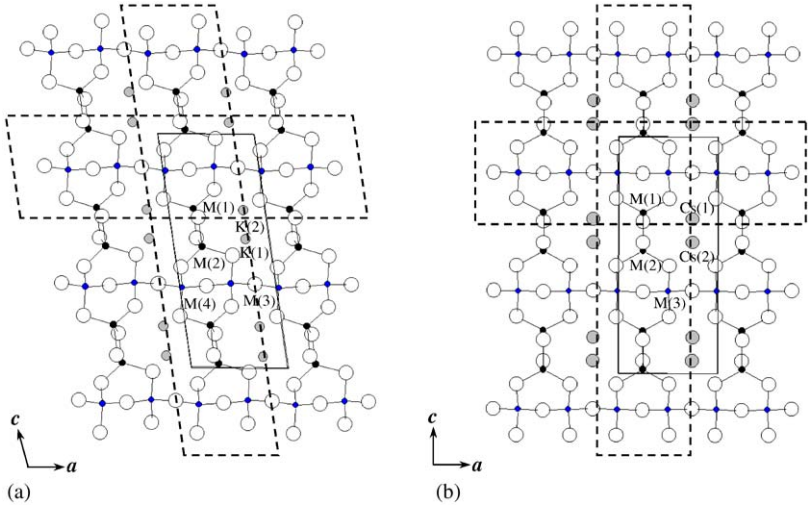

Fig. 4. View perpendicular to the *b*-axis of (a) $KGaSnSe_4$ and (b) $CsGaSnSe_4$, showing a $[GaSnSe_4]^-$ layer. Large open circles are Se atoms, black circles are 4-coordinate (Sn,Ga) atoms, and medium gray circles are K or Cs atoms. The dashed rectangles highlight the one-dimensional chains as a component unit of the layer. *M* represents disordered cation sites for Sn and Ga.

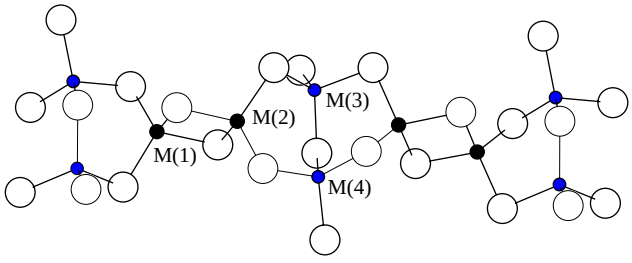

Fig. 5. Geometry of a chain consisting of dimeric $(Sn,Ga)_2Se_6$ and monomeric $(Sn,Ga)Se_4$ units found in $AGaSnSe_4$ (A = K, Rb, and Cs). *M* represents disordered cation sites for Sn and Ga.

There are two non-equivalent positions for alkali-metal atoms. The K atoms in **II** are all coordinated by seven Se atoms with irregular polyhedron geometry. Among the seven K–Se bonds, one K–Se bond has longer distance of 3.849(3) Å for the K(1) and 3.957(3) Å for the K(2), which is much longer than the average of the other bonds : 3.493(3) Å for the K(1) and 3.525(3) Å for the K(2).

In the case of **IV**, the Cs atoms are coordinated by nine Se atoms with irregular polyhedron geometry. While two Se atoms are coordinated to Cs atoms at remote distance of 4.110(2) Å for Cs(1) and 4.017(2) Å for Cs(2), the other seven Cs–Se bond distances range from 3.672(2) to 3.878(1) Å for Cs(1) and from 3.647(2) to 3.839(1) Å for Cs(2).

3.3. Properties

The thermal behavior of $Na_{2-x}Ga_{2-x}Sn_{1+x}Se_6$ (**I**), $KGaSnSe_4$ (α- and β-) (**II**), $RbGaSnSe_4$ (**III**), and $CsGaSnSe_4$ (**IV**) was examined by performing DTA experiments. As shown in Fig. 6a, **I** melts incongruently at 709°C. The powder XRD pattern of **I** was different before and after the DTA experiment (Fig. 6b). The appearance of several new reflections at low diffraction

Table 6
Selected interatomic distances (Å) and angles (deg) for $KGaSnSe_4$

Atoms	Distance	Atoms	Distance
Sn,Ga(1)–Se(2)	2.469(1)	Sn,Ga(1)–Se(4)	2.531(1)
Sn,Ga(1)–Se(7)	2.481(1)	Sn,Ga(1)–Se(8)	2.496(1)
Sn,Ga(2)–Se(4)	2.522(1)	Sn,Ga(2)–Se(5)	2.486(1)
Sn,Ga(2)–Se(6)	2.471(1)	Sn,Ga(2)–Se(8)	2.503(1)
Sn,Ga(3)–Se(1)	2.436(1)	Sn,Ga(3)–Se(2)	2.444(1)
Sn,Ga(3)–Se(3)	2.446(1)	Sn,Ga(3)–Se(5)	2.485(1)
Sn,Ga(4)–Se(1)	2.423(1)	Sn,Ga(4)–Se(3)	2.425(1)
Sn,Ga(4)–Se(6)	2.425(1)	Sn,Ga(4)–Se(7)	2.467(1)
K(1)–Se(1)	3.508(3)	K(1)–Se(3)	3.549(3)
K(1)–Se(4)	3.370(3)	K(1)–Se(4)	3.675(3)
K(1)–Se(4)	3.849(3)	K(1)–Se(5)	3.492(3)
K(1)–Se(7)	3.365(2)		
K(2)–Se(2)	3.512(3)	K(2)–Se(3)	3.387(3)
K(2)–Se(5)	3.779(3)	K(2)–Se(6)	3.312(3)
K(2)–Se(7)	3.614(3)	K(2)–Se(7)	3.957(3)
K(2)–Se(8)	3.548(3)		
Atoms	**Angle**	**Atoms**	**Angle**
Se(2)–Sn,Ga(1)–Se(4)	107.49(4)	Se(2)–Sn,Ga(1)–Se(7)	112.21(4)
Se(2)–Sn,Ga(1)–Se(8)	118.29(4)	Se(4)–Sn,Ga(1)–Se(7)	106.67(4)
Se(4)–Sn,Ga(1)–Se(8)	96.51(4)	Se(7)–Sn,Ga(1)–Se(8)	113.59(4)
Se(4)–Sn,Ga(2)–Se(5)	111.23(4)	Se(4)–Sn,Ga(2)–Se(6)	114.45(4)
Se(4)–Sn,Ga(2)–Se(8)	96.58(4)	Se(5)–Sn,Ga(2)–Se(6)	113.80(4)
Se(5)–Sn,Ga(2)–Se(8)	108.14(4)	Se(6)–Sn,Ga(2)–Se(8)	111.21(4)
Se(1)–Sn,Ga(3)–Se(2)	111.95(4)	Se(1)–Sn,Ga(3)–Se(3)	100.89(4)
Se(1)–Sn,Ga(3)–Se(5)	114.53(4)	Se(2)–Sn,Ga(3)–Se(3)	114.04(4)
Se(2)–Sn,Ga(3)–Se(5)	107.67(4)	Se(3)–Sn,Ga(3)–Se(5)	107.75(4)
Se(1)–Sn,Ga(4)–Se(3)	100.78(5)	Se(1)–Sn,Ga(4)–Se(6)	117.98(4)
Se(1)–Sn,Ga(4)–Se(7)	110.10(4)	Se(3)–Sn,Ga(4)–Se(6)	112.56(4)
Se(3)–Sn,Ga(4)–Se(7)	109.66(4)	Se(6)–Sn,Ga(4)–Se(7)	105.67(5)

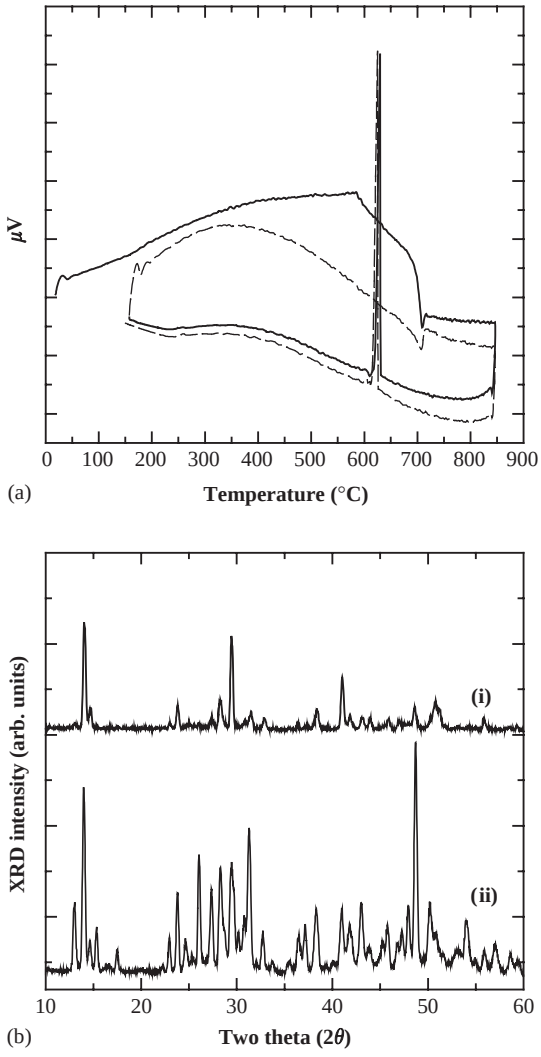

Fig. 6. (a) DTA diagram of $Na_{2-x}Ga_{2-x}Sn_{1+x}Se_6$ and (b) powder XRD patterns for $Na_{2-x}Ga_{2-x}Sn_{1+x}Se_6$ (i) before and (ii) after the DTA experiment. In (a), the solid and dashed lines represent data for the 1st and 2nd heating/cooling cycles, respectively.

angles suggests the formation of a new phase with lower symmetry. Given that the DTA cooling rate is approximately 20 times slower than that applied in the synthesis, the observed change in XRD pattern underlines the fact that **I** a kinetically stable phase.

When α-$KGaSnSe_4$ melts above 649°C and subsequently cools at 10°C/min in a DTA experiment, the crystallized residue is β-$KGaSnSe_4$ according to the XRD pattern. The DTA of **II** (β-), **III**, and **IV** show that these compounds melt congruently at 746°C, 734°C, and 759°C, respectively. In contrast to **I**, the powder XRD patterns for **II** (β-), **III**, and **IV** are unchanged after crystallization of the melt. Upon cooling, they show a sharp exothermic peak corresponding to congruent recrystallization at 661°C, 698°C, and 727°C for **II**, **III**, and **IV**, respectively.

Table 7
Selected interatomic distances (Å) and angles (deg) for $CsGaSnSe_4$

Atoms	Distance	Atoms	Distance
Sn,Ga(1)–Se(4)	2.465(1)	Sn,Ga(1)–Se(5)	2.493(2)
Sn,Ga(1)–Se(6)	2.521(2)		
Sn,Ga(2)–Se(3)	2.456(1)	Sn,Ga(2)–Se(5)	2.492(2)
Sn,Ga(2)–Se(6)	2.487(2)		
Sn,Ga(3)–Se(1)	2.452(1)	Sn,Ga(3)–Se(2)	2.446(1)
Sn,Ga(3)–Se(3)	2.461(2)	Sn,Ga(3)–Se(4)	2.460(2)
Cs(1)–Se(1)	3.672(2)	Cs(1)–Se(3)	3.819(2)
Cs(1)–Se(3)	4.110(2)	Cs(1)–Se(4)	3.872(2)
Cs(1)–Se(5)	3.878(1)		
Cs(2)–Se(1)	3.727(2)	Cs(2)–Se(2)	3.733(2)
Cs(2)–Se(3)	4.017(2)	Cs(2)–Se(4)	3.837(2)
Cs(2)–Se(6)	3.647(2)	Cs(2)–Se(6)	3.839(1)
Atoms	**Angle**	**Atoms**	**Angle**
Se(4)–Sn,Ga(1)–Se(4)	113.14(8)	Se(4)–Sn,Ga(1)–Se(5)	115.91(5)
Se(4)–Sn,Ga(1)–Se(5)	115.91(5)	Se(4)–Sn,Ga(1)–Se(6)	106.35(5)
Se(4)–Sn,Ga(1)–Se(6)	106.36(5)	Se(5)–Sn,Ga(1)–Se(6)	96.78(7)
Se(3)–Sn,Ga(2)–Se(3)	114.32(7)	Se(3)–Sn,Ga(2)–Se(6)	113.14(5)
Se(3)–Sn,Ga(2)–Se(6)	113.14(5)	Se(3)–Sn,Ga(2)–Se(5)	108.52(5)
Se(3)–Sn,Ga(2)–Se(5)	108.52(5)	Se(5)–Sn,Ga(2)–Se(6)	97.71(7)
Se(1)–Sn,Ga(3)–Se(2)	103.34(6)	Se(1)–Sn,Ga(3)–Se(3)	110.14(6)
Se(1)–Sn,Ga(3)–Se(4)	110.94(6)	Se(2)–Sn,Ga(3)–Se(3)	114.91(6)
Se(2)–Sn,Ga(3)–Se(4)	111.48(6)	Se(3)–Sn,Ga(3)–Se(4)	106.11(6)

In the $KInSnSe_4$ system [13], we observed that on annealing the α- and the β-phases just below the melting point, they convert to a third γ-form which has a three-dimensional framework belonging to the $BaGa_2S_4$ structure type, Fig. 7a. We therefore decided to perform annealing experiments on the $AGaSnSe_4$ compounds as well to check for similar transitions. Accordingly, α-$KGaSnSe_4$, $RbGaSnSe_4$ and $CsGaSnSe_4$ were annealed in a furnace at 650°C for 48 h. On cooling the solids to room temperature at the rate of 10°C/h, we found that α-$KGaSnSe_4$ and $RbGaSnSe_4$ had indeed converted to the cubic γ-form. Since α-$KGaSnSe_4$ melts at 649°C, this transformation from α to γ occurs via the formation of the β phase. Fig. 7b compares the powder patterns of the gamma forms of $KGaSnSe_4$ and $RbGaSnSe_4$ with γ-$KInSnSe_4$. We were unable to obtain suitable single crystals for structure determination. However from the figure, it is clear that both γ-$KGaSnSe_4$ and $RbGaSnSe_4$ are isostructural to γ-$KInSnSe_4$. From these observations we conclude that the γ-form is the true thermodynamically stable product. Therefore, in these systems cooling of melts only leads to kinetically stable products. If the annealing step is not performed it is easy to incorrectly identify one of them as the thermodynamically stable one.

Optical absorption spectra (Fig. 8) indicate that all compounds are wide band gap semiconductors. The band gap was estimated to be 1.50, 1.73, 1.88, and 1.97 eV for **I**, **II**, **III**, and **IV**, respectively, which are

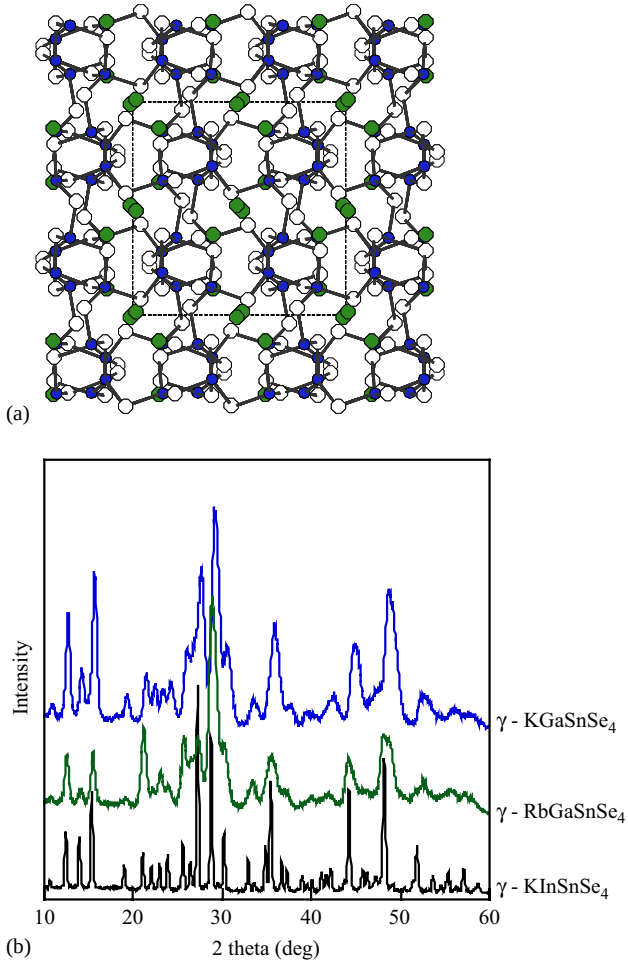

Fig. 7. (a) The three-dimensional framework of (cubic $BaGa_2S_4$-type) γ-$KInSnSe_4$ (cubic $BaGa_2S_4$-type) and (b) Comparison of the powder patterns of the cubic γ-forms of $KGaSnSe_4$, $RbGaSnSe_4$ and $KInSnSe_4$ shows that they are isostructural.

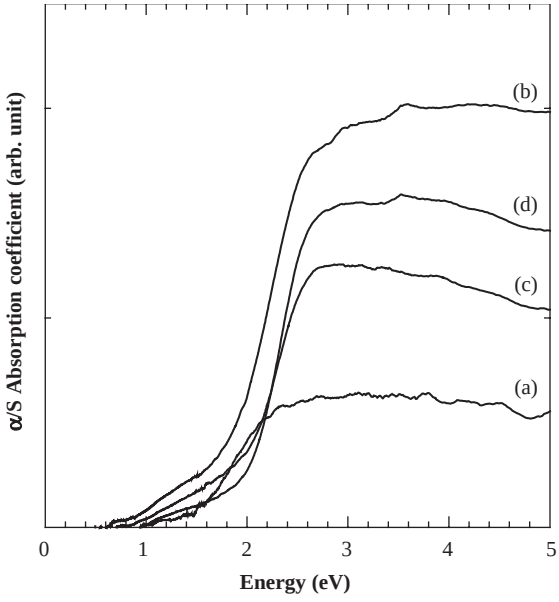

Fig. 8. UV/Vis absorption spectra for: (a) $Na_{2-x}Ga_{2-x}Sn_{1+x}Se_6$, (b) $KGaSnSe_4$, (c) $RbGaSnSe_4$, and (d) $CsGaSnSe_4$.

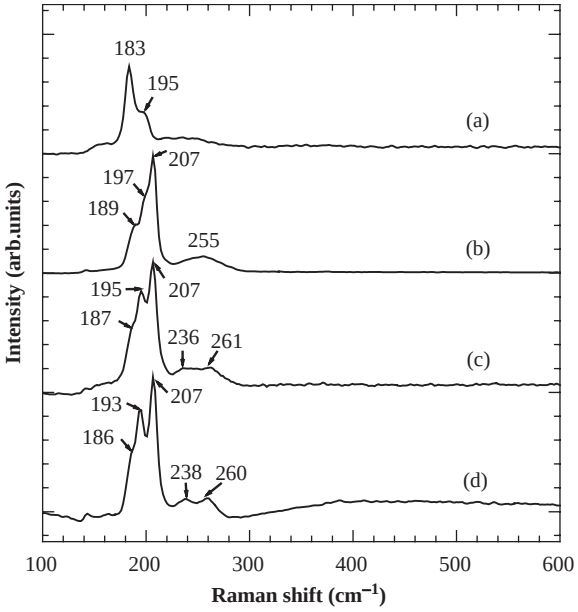

Fig. 9. FT Raman spectra for crystals of: (a) $Na_{2-x}Ga_{2-x}Sn_{1+x}Se_6$, (b) $KGaSnSe_4$, (c) $RbGaSnSe_4$, and (d) $CsGaSnSe_4$.

similar to the band gaps of $K_2MnSn_2Se_6$ (2.0 eV), $K_2MnSnSe_4$ (1.7 eV), and $K_2Ag_2SnSe_4$ (1.8 eV) [10].

Raman spectra of crystals recorded between 100 and 600 cm^{-1} for all compounds, are presented in Fig. 9. The spectral patterns of **II**, **III**, and **IV** are similar to one another, showing a number of strong peaks between 150 and 300 cm^{-1} with a maximum at 207 cm^{-1}. Raman peaks originating from Ga–Se bonds in β-Ga_2Se_3 were observed in this frequency range [20]. Additional peaks are observed at 197 (s) and 189 (m) cm^{-1} for **II**, 195 (s) and 187 (m) cm^{-1} for **III**, and 193 (s) and 186 (m) cm^{-1} for **IV**, respectively (s = strong, m = medium). These compounds also have several weaker and broader features between 220 and 270 cm^{-1}.

Consistent with its different structure type, **I** shows different somewhat simpler Raman spectral features from **II**, **III**, and **IV**. Only two intense peaks are observed at 183 and 195 cm^{-1} for this compound, which may be due to the fact that it contains only corner-shared tetrahedra whereas the other compounds contain both corner- and edge-shared tetrahedra.

4. Conclusion

The quaternary selenostannates, $Na_{2-x}Ga_{2-x}Sn_{1+x}Se_6$ and $AGaSnSe_4$ (A = K, Rb, and Cs), were prepared with a flame melting–rapid cooling method. The structure of $Na_{2-x}Ga_{2-x}Sn_{1+x}Se_6$ can be described as three-dimensional polar network of trimeric $(Sn,Ga)_3Se_9$ units with Na atoms in one-dimensional tunnel. This phase is found to require a fast crystallization condition to form and it is regarded to be only kinetically stable. In light of

this, it is evident that the flame melting–rapid cooling method is a potent technique of synthesizing and crystallizing kinetically stable forms that often cannot be prepared by conventional slow cooling processes. Although quenching is a well-known technique for stabilizing kinetically stable phases, what is attractive here is that usable single crystals are obtained readily and without further processing or recrystallization procedures. Using the same technique we prepared a kinetically stable form of $KInSnSe_4$ and found that it transforms to the thermodynamically stable form during heating [13]. On the other hand, α-$KGaSnSe_4$ and $RbGaSnSe_4$ transform to the thermodynamically stable γ-forms on heating, but $CsGaSnSe_4$ remains unchanged. Presumably a kinetically stable compound does not exist in the Cs system. Remarkably however in the K and Rb analogs, the true thermodynamically stable form is the γ-form which is not accessible by cooling the melts. Given that extended annealing of phases is rarely performed, the results of this work have greater implications in that many reported phases prepared by cooling of melts may in fact be only kinetically stable. The true thermodynamically stable phases could lay hidden and inaccessible unless proper annealing is performed to uncover them.

Acknowledgments

Financial support from the National Science Foundation (DMR-0127644) is gratefully acknowledged. This work was supported in part by Korea Research Foundation Grant (KRF-2003-042-C00065).

References

[1] M.G. Kanatzidis, A.C. Sutorik, Prog. Inorg. Chem. 43 (1995) 151.
[2] (a) B. Krebs, Angew. Chem. Int. Ed. Engl. 22 (1983) 113;
(b) J. Olivier-Fourcade, J.C. Jumas, M. Ribes, E. Philippot, M. Maurin, J. Solid State Chem. 23 (1978) 155;
(c) M. Ribes, Rev. Chim. Miner. 7 (1970) 75;
(d) C.R. Evenson, P.K. Dorhout, Inorg. Chem. 40 (10) (2001) 2409–2414;
(e) D. Johrendt, Acta Crystallogr. E 58 (2002) I52–I55;
(f) O. Palchik, A. Gedanken, V. Palchik, M.A. Slifkin, A.M. Weiss, J. Solid State Chem. 165 (1) (2002) 125–130.
[3] (a) W.S. Sheldrick, M. Wachhold, Coord. Chem. Rev. 176 (1998) 211–322;
(b) A. Loose, W.S. Sheldrick, J. Solid State Chem. 147 (1) (1999) 146–153.
[4] K. Susa, H. Steinfink, J. Solid State Chem. 7 (1971) 75.
[5] W. Schiwy, S. Pohl, B. Krebs, Z. Anorg. Allg. Chem. 402 (1973) 77.
[6] B. Krebs, W. Schiwy, Z. Anorg. Allg. Chem. 393 (1973) 63.
[7] S. Pohl, B. Krebs, Z. Anorg. Allg. Chem. 424 (1976) 265.
[8] J.H. Liao, C. Varotsis, M.G. Kanatzidis, Inorg. Chem. 32 (1993) 2453.
[9] J.H. Liao, M.G. Kanatzidis, Chem. Mater. 5 (1993) 1561.
[10] X. Chen, X. Huang, A. Fu, J. Li, L.D. Zhang, H.Y. Guo, Chem. Mater. 12 (2000) 2385.
[11] J.D. Breshears, M.G. Kanatzidis, J. Am. Chem. Soc. 122 (2000) 7839.
[12] (a) T. Kyratsi, K. Chrissafis, J. Wachter, K.M. Paraskevopoulos, M.G. Kanatzidis, Adv. Mater. 15 (2003) 1428;
(b) K. Chrissafis, T. Kyratsi, K.M. Paraskevopoulos, M.G. Kanatzidis, Chem. Mater. 16 (2004) 1932.
[13] S.J. Hwang, R.G. Iyer, P.N. Trikalitis, A.G. Ogden, M.G. Kanatzidis, Inorg. Chem. 43 (2004) 2237.
[14] (a) J.A. Aitken, G.A. Marking, M. Evain, L. Iordanidis, M.G. Kanatzidis, J. Solid State Chem. 153 (2000) 158;
(b) F. Feher, Handbuch der Präparativen Anorganischen Chemie, in: G. Brauer (Ed.), Vol. 1, Ferdinand Enke, Stuttgart, Germany, 1954, pp. 280–281.
[15] G.A. Marking, J.A. Hanko, M.G. Kanatzidis, Chem. Mater. 10 (1998) 1191.
[16] (a) SMART, Version 5; Siemens Analytical X-ray systems, Inc.; Madison, WI, 1998;
(b) SAINT, Version 4; Siemens Analytical X-ray systems, Inc., Madison, WI, 1994–1996;
(c) G.M. Scheldrick, SADABS;SHELXTL, Siemens Analytical X-ray systems, Inc., Madison, WI, 1997.
[17] H.Y. Hong, H. Steinfink, J. Solid State Chem. 5 (1972) 93.
[18] Y. Nakamura, A. Aruga, I. Nakai, K. Nagashima, Bull. Chem. Soc. Japan 57 (1984) 1718.
[19] P. Wu, Y.J. Lu, J.A. Ibers, J. Solid State Chem. 97 (1992) 383.
[20] M. Takumi, Y. Koshio, K. Nagata, Phys. Stat. Sol. (b) 211 (1999) 123.